FEATURE ARTICLE

Predictive Theory for Hydrogen Atom−Hydrocarbon Radical Association Kinetics

Lawrence B. Harding*

Chemistry Division, Argonne National Laboratory, Argonne, Illinois 60439

Yuri Georgievskii and Stephen J. Klippenstein

Combustion Research Facility, Sandia National Laboratory, Livermore, California 94551-0969

Received: February 18, 2005; In Final Form: March 31, 2005

Procedures for accurately predicting the kinetics of hydrogen atom associations with hydrocarbon radicals are described and applied to a series of reactions. The approach is based on CASPT2/cc-pvdz evaluations of the orientation-dependent interaction energies within variable reaction coordinate transition state theory. One-dimensional corrections to the interaction energies are estimated from CAS+1+2/aug-cc-pvtz evaluations for the H + CH_3 reaction, and a dynamical correction factor of 0.9 is applied. This corrected CASPT2 approach yields results that are within 10% of those obtained with the full CAS+1+2/aug-cc-pvtz potential for the H + CH_3, H + C_2H_5, H + C_2H_3, and H + C_2H reactions. New predictions are made for the H + *iso*-C_3H_7, H + *tert*-C_4H_9, H + C_6H_5, and H + $C_{10}H_7$ reactions. For the H + CH_3 and H + C_2H_3 reactions, where the experimental values appear to be the most well-determined, theory and experiment essentially agree to within their error bars. For the other reactions, the agreement is reasonably satisfactory given the often large dispersion in the experimental results. For the reactions with saturated alkyl radicals, the theory predicts that each additional CH_3 group increases the steric factor by approximately a factor of 2. In contrast, for the unsaturated radicals, the H + C_6H_5 and H + $C_{10}H_7$ high-pressure association rate coefficients are nearly identical to that for H + C_2H_3.

1. Introduction

The simplest of the hydrogen atom−hydrocarbon radical association reactions

$$H + CH_3 \rightarrow CH_4 \quad (1)$$

has been an important benchmark for the study of radical−radical association reactions. It is known to be of importance in the chemistry of both hydrocarbon combustion[1] and planetary atmospheres.[2] Its rate has been measured in both the forward[1,3−5] and the reverse directions.[6−11] Studies of isotopically substituted reactions[1,4,5] have provided definitive data for the high-pressure limit. There have also been numerous theoretical studies of this reaction, including ab initio studies of the potential surface[12−21] together with statistical adiabatic channel model,[22−27] Gorin model,[28] transition state theory,[14,19,21,29−36] quasiclassical trajectory,[21,33,37−39] and quantum dynamics[40] studies of the kinetics. As a consequence, the temperature dependence of the high-pressure association rate coefficient for this reaction is fairly well-understood.

The number of reported studies of hydrogen atom reactions with larger hydrocarbon radicals (both experimental and theoretical) drops precipitously as the size of the radicals increases. Consider, for example, the prototypical series of hydrogen atom associations with primary, secondary, and tertiary alkyl radicals in reactions 2−4

$$H + C_2H_5 \rightarrow C_2H_6 \quad (2)$$

$$H + \textit{iso}\text{-}C_3H_7 \rightarrow \textit{n}\text{-}C_3H_8 \quad (3)$$

$$H + \textit{tert}\text{-}C_4H_9 \rightarrow \textit{iso}\text{-}C_4H_{10} \quad (4)$$

Ten measurements have been reported[41−50] on the rate of reaction 2. All are at relatively low temperatures, and there is large scatter in the data (the two most recent of these measurements differ by approximately a factor of 3 at room temperature). Only one measurement for reaction 3 has been reported,[51] and no measurements have been reported for reaction 4. Reaction 2 is thought to be the most important loss process for C_2H_5 in the atmospheres of Jupiter and Saturn. Models of the chemistry of these atmospheres require low-temperature rate data; however, only one low-temperature measurement has been reported[50] for reaction 2.

There have also been numerous experimental studies of the related dissociations, which are directly related to the association rate coefficients through the equilibrium constant. However, in this overview article, we shall consider only the direct associa-

* Author to whom correspondence should be addressed. Phone: (630) 252-3591. Fax: (630) 252-9292. E-mail: harding@anl.gov.

10.1021/jp0508608 CCC: $30.25
Published on Web 04/22/2005

tion rate coefficient measurements, to avoid any ambiguities related to the properties of the equilibrium constant. Consideration of the dissociation measurements is more appropriate in the context of a complete analysis of the pressure dependence of the kinetics.

Aside from the importance of these reactions in combustion chemistry and planetary atmospheres, reactions 1−4 are of more fundamental interest. Early attempts to rationalize the rates of radical−radical associations involved comparing the observed rate coefficients to calculated collision frequencies and attributing the difference to steric factors.[52] Attempts were then made to analyze these steric factors in terms of overlap (or lack thereof) between the two radical orbitals for particular orientations and in terms of excluded volumes caused by Pauli principle repulsions involving bond pairs adjacent to the radical sites. These efforts were hampered by the lack of accurate rate data. Although more of this rate data is now available, the lack of data for the largest radical in the series of reactions 1−4 and uncertainties in the rates for reactions 2 and 3 continue to make this kind of empirical analysis problematic. For these reasons, our understanding of steric factors in these association reactions is still incomplete.

Association reactions involving unsaturated hydrocarbon radicals are also of potential importance in combustion and planetary atmospheres. The simplest of these are reactions 5 and 6.

$$H + CCH \rightarrow HCCH \quad (5)$$

$$H + C_2H_3 \rightarrow C_2H_4 \quad (6)$$

Measurements on reaction 5 have only been reported for the reverse reaction[53−55] although there have been previous theoretical studies in both directions.[56,57] A number of measurements have been reported[58−62] for reaction 6 in the forward direction (see also the recent review by Laufer and Fahr[63]). It has been noted[64] that reaction 6 is an important chain-terminating step in the pyrolysis of ethane. For association reactions involving unsaturated radicals, there has been some discussion as to the possible participation of triplet surfaces[60] although theoretical studies[65] have shown that this is not likely, at least for reaction 6.

In a previous series of papers, we presented theoretical analyses of the reactions $H + CH_3$,[21] $H + C_2H_3$,[65] and $H + C_2H_5$.[66] These studies employed large basis set, ab initio, multireference, configuration interaction (CAS+1+2) calculations to characterize the potential surfaces together with variable reaction coordinate transition state theory (VRC-TST)[67,68,69] to calculate the high-pressure-limit rate coefficients. Although this approach yields reliable predictions, it cannot be readily applied to larger systems due to the poor scaling properties of CAS+1+2 calculations. In this paper, we demonstrate that the combination of small basis set, second-order, multireference perturbation theory (CASPT2) calculations together with a simple one-dimensional (1D) correction yields potential surfaces of comparable accuracy to those from the large basis set CAS+1+2 calculations in the kinetically significant regions for these reactions. The key advantage of the CASPT2-based approach is that the superior scaling properties of CASPT2 versus CAS+1+2 allow calculations on much larger systems.

The outline of this paper is as follows; in the next section, we describe the details of the electronic structure and VRC-TST methods used. In section 3.1 we report calculations on four association reactions 1, 2, 5, and 6, each of which involve only two heavy atoms. Here, we compare potential surfaces and kinetics obtained using both large basis set CAS+1+2 and the new, corrected, small basis set CASPT2 approach. These comparisons demonstrate that the corrected CASPT2 potential surfaces are sufficiently accurate for the calculation of the high-pressure association rate coefficients. In section 3.2, we then report new predictions for some sample larger systems, specifically reactions 3, 4, and 7−9

$$H + C_6H_5 \rightarrow C_6H_6 \quad (7)$$

$$H + 1\text{-}C_{10}H_7 \rightarrow C_{10}H_8 \quad (8)$$

$$H + 2\text{-}C_{10}H_7 \rightarrow C_{10}H_8 \quad (9)$$

for which large basis set multireference configuration interaction calculations are not readily feasible.

2. Methods

2.1. Electronic Structure Methods. As described in the Introduction, we report two levels of electronic structure calculations, large basis set CAS+1+2 and small basis set CASPT2. The CAS reference spaces for both calculations are identical. Specifically, we use the smallest complete active space (CAS) reference space that yields a qualitatively correct description (no spurious ionic character and no spin contamination) of the reactant asymptote. For all of the reactions studied here, a two-electron, two-orbital CAS reference space satisfies this criterion.

The CAS+1+2 calculations employ the Dunning[70] aug-cc-pvtz basis set and the internal contraction formalism of Werner and Knowles.[71,72] A multireference, Davidson correction is used to correct for the neglect of higher-order excitations. The CASPT2 calculations employ the Dunning[73] cc-pvdz basis sets and the formalism of Celani and Werner.[74] The MOLPRO program package[75,76] was used for both the CAS+1+2 and the CASPT2 calculations.

As discussed in the next section, the transition state theory method used here neglects changes in the internal degrees of freedom of the reactants, i.e., the geometries of the hydrocarbon radicals are kept fixed at their asymptotic, equilibrium geometries. With this approximation all of the hydrogen + hydrocarbon radical association reactions can be treated using three-dimensional potential surfaces where the three dimensions correspond to motions of the hydrogen atom relative to the rigid, fixed hydrocarbon radical. The kinetic predictions are only weakly dependent on the equilibrium geometries of these radicals and so they were simply determined from B3LYP/6-31G* calculations using the GAUSSIAN98 program.[77]

In Figure 1, we compare one-dimensional potential curves for $H + CH_3$ calculated using the CAS+1+2/aug-cc-pvtz and CASPT2/cc-pvdz methods. Both curves are calculated assuming the H atom approaches along the C_3 axis of the CH_3 radical. In Figure 2, we plot the difference between these two potential curves. From these plots, it can be seen that the CAS+1+2/aug-cc-pvtz potential curve is approximately 20% more attractive than the CASPT2/cc-pvdz curve in this kinetically sensitive, long-range region. It should be noted that this difference is almost entirely due to the difference in basis sets, cc-pvdz vs aug-cc-pvtz, not to the difference in methods, CASPT2 vs CAS+1+2. This ~20% difference in the attractiveness of these two potentials will translate into an ~20% difference in the room-temperature association rate coefficients calculated using these two potentials (see below).

To correct the cc-pvdz calculations for this basis set deficiency, we will make two key approximations. First, we assume that the difference potential shown in Figure 2, although calculated for approach along the C_3 axis of CH_3, is, to a

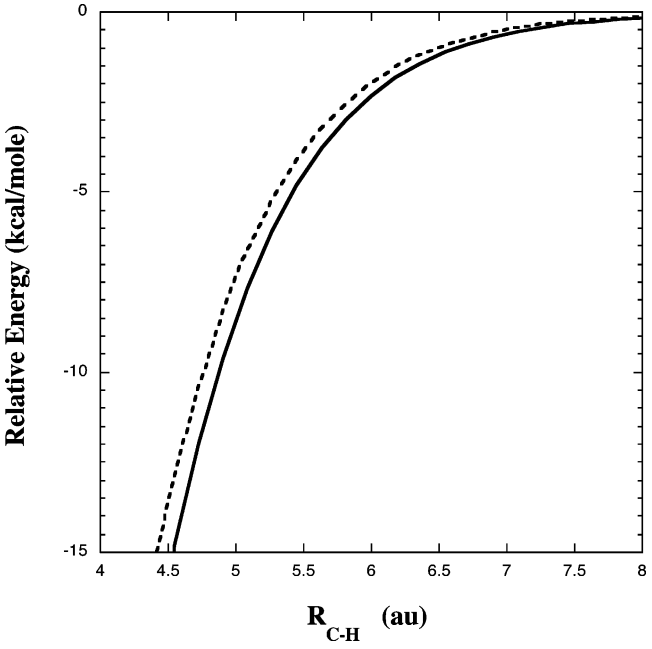

Figure 1. Potential curves for H + CH_3. The solid line corresponds to CAS+1+2/aug-cc-pvtz and the dashed line to CASPT2/cc-pvdz.

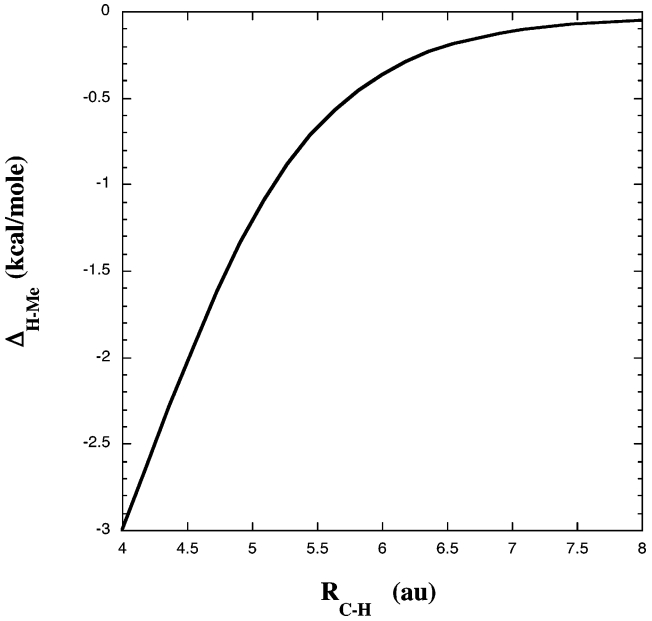

Figure 2. Difference potential curve for H + CH_3, $\Delta_{H-Me} = V_{CAS+1+2/aug\text{-}cc\text{-}pvtz} - V_{CASPT2/cc\text{-}pvdz}$.

reasonable approximation, independent of orientation. The second approximation is that the same difference potential, evaluated for H + CH_3, can be used to correct any CASPT2/cc-pvdz, hydrogen atom + hydrocarbon radical, association potential. With these two approximations we then define the potential, *V*, for a hydrogen atom interacting with an arbitrary, rigid, hydrocarbon radical as follows

$$V(R,\theta,\phi) = V_{CASPT2/cc\text{-}pvdz}(R,\theta,\phi) + \Delta_{H+Me}(R) \quad (10)$$

where $V_{CASPT2/cc\text{-}pvdz}(R,\theta,\phi)$ is the three-dimensional CASPT2/cc-pvdz potential for a hydrogen atom interacting with the hydrocarbon radical, *R* is the distance between the hydrogen atom and the closest radical carbon atom, θ and ϕ are the two orientational degrees of freedom of the three-dimensional potential, and Δ_{H+Me} is the difference between the CAS+1+2/aug-cc-pvtz and CASPT2/cc-pvdz potentials for H + CH_3 calculated for approach along the C_3 axis of the rigid CH_3 radical (Figure 2). The justification for this definition will be given in sections 3.1.1−3.1.4 where we will compare high-pressure-limit, TST association rate coefficients for four reactions calculated using both potentials defined by eq 10 and potentials derived directly from CAS+1+2/aug-cc-pvtz calculations.

2.2. Transition State Theory Methods. For barrierless reactions, the transition state varies greatly with energy and with angular momentum, with these variations making it relatively difficult to obtain accurate a priori predictions for the association rate coefficients.[78] In the following qualitative discussion, for simplicity, we will focus on the temperature dependence of the properties of the transition state. However, it is important to recognize that an accurate accounting of the energy and angular-momentum dependence of the transition state properties is a prerequisite to making accurate TST predictions. Thus, the present analyses are all performed at the energy and angular-momentum-resolved level.

There are two key aspects to the variations in the transition state. Typically, one focuses on the variation in the separation between the two reacting fragments, which generally varies from tens of angstroms at low temperatures to about 2−4 Å at higher temperatures. However, the variation in the shape or form of the transition state dividing surface is in reality just as important. At low temperature, where the fragment−fragment separation in the transition state is large, the distance between the centers of mass of the two fragments provides a good representation of the reaction coordinate and thus the shape of the dividing surface. At shorter separations, as chemical bonding begins to develop, a fixed separation between the centers of the radical orbitals on each of the fragments provides a better first approximation to the transition state dividing surface.

With the variable reaction coordinate approach, the dividing surfaces are defined in terms of a fixed distance between pivot points on each of the fragments.[67,68,79−81] These pivot points define the origins of the fragment rotations within the transition state dividing surface. Both the location of the pivot points and the separation between them are varied in determining a variational minimum for the TST rate coefficient. When the pivot points are placed at the centers of mass of the fragments, one obtains an approach that is appropriate at large separations. When the pivot points are placed near the center of the radical orbitals, one obtains an approach that is appropriate at short separations. Thus, the variable reaction coordinate approach provides a unified treatment of the two quite distinct transition state regions and thus for the full range of temperatures.

For each of the reactions considered here, the pivot point for the hydrogen atom is simply taken to be its center of mass. The situation for the polyatomic hydrocarbon radicals is considerably more complex. The hydrogen atom can often add to these radicals from two different sides. For radicals in which the radical center is nonplanar, the two sides of the radical are not equivalent, and we refer to the convex side as the "front" and the concave side as the "back" It can then be important to have an independent optimization of the shape of the dividing surface for the different sides of attack. A recent generalization of the variable reaction coordinate approach accomplishes this independent optimization by placing multiple pivot points on each of the fragments.[69,80] A multifaceted dividing surface is then generated from the consideration of a set of fixed distances between each pair of pivot points (with one part of the pair on each of the fragments). An alternative approach, which is conceptually less satisfactory since it can violate the variational

principle, is based on the assumption of infinite potentials separating the different binding sites.[65,68,69,82] The addition rate to the different binding sites can then be evaluated separately, with the total rate simply given by the sum of those for the individual sites.

An H atom can add to either of the two identical faces of the CH_3 radical. Thus, the multifaceted dividing surface approach considers two separate pivot points for the CH_3 radical, one for each face. Meanwhile, for the H atom, the pivot point is simply taken to lie at its nucleus. The equivalence of the two faces of the methyl radical implies that the two pivot points are symmetrically related for any *E*, *J* combination. This symmetry also implies that, for the $CH_3 + H$ reaction, the infinite potential and multifaceted dividing surface results are identical. For either approach, the variational optimization involves the minimization of the rate coefficient with respect to two coordinates, the distance *d* specifying the location of the CH_3 pivot points relative to the C atom along its C_3 axis and the distance *r* specifying the separation between the two pivot points.

For the vinyl radical and most of the other radicals, the hydrogen atom can again add from either the front or the back. In addition, there is a barrierless pathway leading to the abstraction of a hydrogen atom. Thus, three pivot points are considered for the C_2H_3 radical. Symmetry implies that these three pivot points can be taken to lie in the plane of the C_2H_3 radical. However, in this case, the sides are not equivalent, and a complete multifaceted dividing surface analysis should jointly optimize nine parameters. These nine parameters consist of a distance and orientation relative to the radical C atom for each of the C_2H_3 pivot points and separate distances between the H atom and each one of these C_2H_3 pivot points. In contrast, the infinite potential approach separates the analysis into three separate evaluations, with three parameters to be optimized for each one.

The two approaches were found to yield similar results (within ~5%) in a related study of the $C_3H_3 + H$ reaction[69] and in preliminary studies of a number of the present reactions. Thus, the infinite potential approach, which is, of course, much more efficient, was followed in generating the final results presented here. However, it is worth noting that the multifaceted dividing surface approach can generally be made tractable via simple restrictions in the optimization space. For example, the pivot point to pivot point separations for different faces may be assumed to have a constant difference.

The variable reaction coordinate approach is based on a separation of modes into the internal vibrational modes of the fragments, termed the conserved modes, and the remaining "transitional" modes, which correlate with the rotations and relative translations of the fragments. A classical treatment for the latter modes suffices, due to their low-frequency nature. The full transition state partition function may be obtained from a convolution of the classical result for the transitional modes with a direct sum over the quantized energy levels for the conserved modes.

However, under certain limiting conditions, the conserved mode contribution to the transition state partition function is canceled by the analogous contribution to the reactant partition function within the high-pressure-limit rate coefficient. In particular, this cancellation arises when the conserved modes are considered to be adiabatic and to be unchanged from their separated fragment values.[83] Studies of the vibrational distributions in photodissociation experiments suggest that the conserved modes are indeed adiabatic from the transition state to separated products.[84,85] However, at shorter separations, geometrical relaxations of the fragment structures do arise, and the conserved mode frequencies do vary. The geometrical relaxations yield a decrease in the potential and a corresponding increase in the rate coefficient, while the vibrational frequencies typically increase with decreasing separation yielding a decrease in the rate coefficient. The canceling effect of these two variations mitigates their significance to some extent. For simplicity, these two effects will be ignored in all of the present calculations, and the conserved mode contributions will be assumed to cancel.

Nevertheless, it is worth noting that, at very high temperatures, e.g., above about 2000 K, the transition state occasionally moves in to such short separations that the minimum in the flux disappears and the rate goes smoothly to zero with decreasing separation. This disappearance of the minimum is an artifact of the neglect of the relaxation of the conserved modes. The conserved mode relaxation energy becomes significant at about 4 bohr. The inclusion of the relaxation energy has the effect of constraining the optimal dividing surfaces to lie at larger separation. Sample calculations suggest that simply constraining the dividing surface to lie at about 4 bohr or larger, as is done here, provides an effective approximate solution to the neglect of the relaxation effects. For the present reactions, the net effect is an ambiguity of about 5% in the estimated rate coefficient at 2000 K. A more detailed consideration of these factors will be provided in a future study. Note, however, that these effects are expected to be more important in reactions with weak attractions, such as those that occur with resonantly stabilized radicals, and in reactions with greater steric effects, such as those that occur with two polyatomic reactants.

In some cases, for example, $C_2H_5 + H$, the front and back additions appear to become equivalent when certain low-frequency internal modes (e.g., the umbrella bending and/or torsional modes) of the radical fragment are allowed to relax. In this instance, one might assume that the front rate should simply be multiplied by a factor of 2. However, this assumption is in fact incorrect, as the potential for these internal mode(s) of the radical also changes from its form at infinite separation. A proper treatment should consider the joint partition function for these internal mode(s) and transitional modes (including both front and back). The accurate evaluation of this joint partition function is generally too complex. Nevertheless, it may be reasonably approximated as the sum of the transitional mode partition functions for the front and back times the partition function for these internal mode(s).[86] In the transition state, the contribution to this joint partition function from the internal mode(s) effectively cancels with their contribution to the reactants partition function. Thus, the proper effective transitional mode partition function at the transition state is the sum of those for the front and back additions.

With these simplifications, the implementation of the variable reaction coordinate approach to a given reaction just requires an interaction potential for arbitrary separation and orientation of the two reacting fragments. The determination of this potential from CASPT2 and CAS+1+2 calculations was described in the preceding subsection. For the present case of the addition of an atom to a radical, it is relatively straightforward to generate analytic forms for these interaction potentials from fits to ab initio calculations on a grid of data points. This fitting has been performed for the CAS+1+2 surfaces, while for the CASPT2 surfaces we have mostly evaluated the interaction energies on the fly.

In either case, we evaluate the configurational integrals via Monte Carlo integration over the orientational coordinates. These

integrations are done on parallel workstation clusters with the Monte Carlo sampling terminated when the predicted error bars are below a given threshold. For the cases with analytic potentials and the four test reactions, these error bars were chosen to be on the order of 1−2%. For most of the larger reactions, where the interaction energies were generated on the fly, errors bars of 5% were deemed acceptable. For the H + naphthyl reactions, errors bars of 10% were employed.

Pivot point to pivot point separations ranging from about 4 bohr to about 15 bohr were considered. At short separations, grid spacings of 0.5 bohr were employed, and the pivot points were located in the neighborhood of the radical orbital center. The pivot point locations were optimized on a 0.5 bohr grid, with optimal displacements from the radical ranging from 0 to 2 bohr. An optimal displacement of 1.5−2.0 bohr in the direction of the radical orbital was found to be most typical, as was found in earlier studies.[21,65,66] These locations reinforce the view that the optimal dividing surfaces are closely related to the contours of the radical orbital.[65]

At larger separations (8 bohr and greater), where the dependence on separation is weaker, spacings were gradually increased to up to 2 bohr, and the pivot point was placed at the radical center of mass. Some overlap in the short- and long-range descriptions was incorporated by considering both sets of pivot points in the 8−9 bohr region.

With these grid parameters, we expect minimization errors of about 5% or less. The infinite potentials employed to separate the front, back, and abstraction channels were obtained from consideration of the contour plots of the potential energy surface. The abstraction channel is ignored here to focus solely on the association rates. In some instances, it does, however, contribute significantly to the overall reaction rate, for example, for the *tert*-butyl + H reaction.

In prior work, we have examined the kinetics of a number of H atom addition reactions (e.g., H + CH_3,[21] H + C_2H_3,[68] H + C_3H_3,[69] H + C_3H_5, H + CH_3O,[87] etc.) with trajectory simulations. These trajectory simulations suggest that the best VRC-TST predictions tend to overestimate the rate coefficient by about 10%. Thus, each of the calculations presented here employs a uniform dynamical correction factor of 0.9.

3. Results and Discussion

3.1. Tests of Corrected CASPT2/cc-pvdz Calculations for Small Systems. The focus of this section will be a comparison of CAS+1+2/aug-cc-pvtz and corrected CASPT2/cc-pvdz potential surfaces and of VRC-TST association rate coefficients calculated using these surfaces. The four hydrocarbon radicals chosen for this comparison, CH_3, C_2H_5, C_2H_3, and C_2H, are of very different character, having radical orbitals of pure p, sp^3, sp^2, and sp hybridization, respectively. As described above, the same 1D correction will be used for all four reactions to allow the application of this approach to large radicals. This 1D correction is based solely on the H + CH_3 potential.

3.1.1. H + CH_3 → CH_4. In Figure 3, we show a two-dimensional contour plot of the CAS+1+2/aug-cc-pvtz potential for H + CH_3. This can be compared to the contour plots in Figures 4a and 4b in which we show the corresponding CASPT2/cc-pvdz potential and the difference between the CAS+1+2/aug-cc-pvtz and CASPT2/cc-pvdz potentials, respectively. These plots demonstrate that although the CASPT2/cc-pvdz potential is not as attractive as the CAS+1+2/aug-cc-pvtz potential, in all other respects, the shapes of the two potentials are quite similar. The corrected CASPT2/cc-pvdz potential for this system, as defined by eq 10, is shown in Figure 5a, and the difference between this potential and the CAS+1+2/aug-cc-pvtz potential is shown in Figure 5b. From Figure 5b, it can be seen that the only part of the corrected CASPT2/cc-pvdz potential that differs from the CAS+1+2/aug-cc-pvtz potential by more than 1 kcal/mol is in the repulsive regions where the H atom is approaching in, or close to, the plane of the CH_3 radical. In this region, which is of little relevance to the kinetic estimates, the corrected CASPT2 potential is slightly less repulsive than the more accurate CAS+1+2 potential.

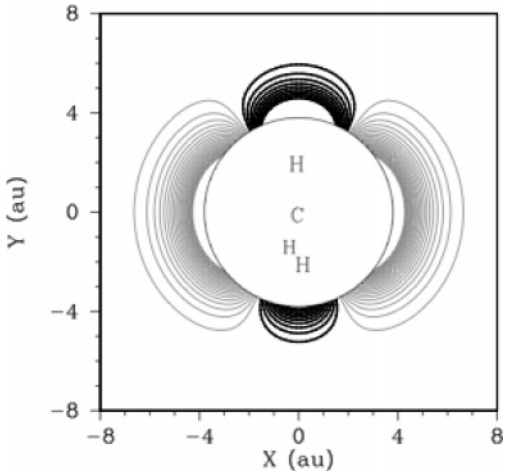

Figure 3. Two-dimensional contour plot of the three-dimensional CAS+1+2/aug-cc-pvtz potential surface for the H + CH_3 → CH_4 association reaction. The plotting plane is perpendicular to the plane of the molecule, includes one CH bond, and bisects the other two CH bonds. The heavier contours denote positive energies, and the lighter contours denote negative energies. Zero energy is defined to be the energy of the H + CH_3 asymptote. The contour increment is 1 kcal/mol. All distances are in atomic units (1 au = 0.52918 Å). The blank circle in the center hides parts of the surface that are not relevant to the association kinetics and were therefore not calculated.

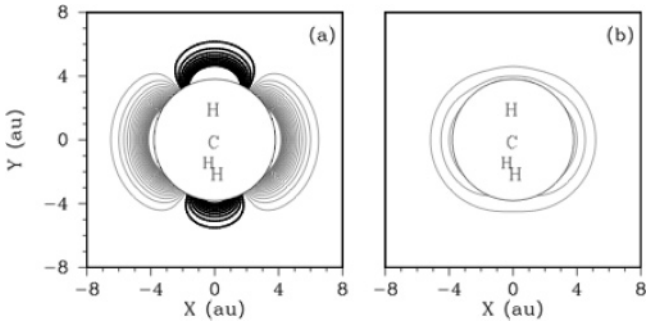

Figure 4. Potential and difference potential surfaces for H + CH_3 → CH_4. (a) CASPT2/cc-pvdz potential surface. (b) The difference potential, CAS+1+2/aug-cc-pvtz minus CASPT2/cc-pvdz. Plotting conventions for both part a and part b are as in Figure 3.

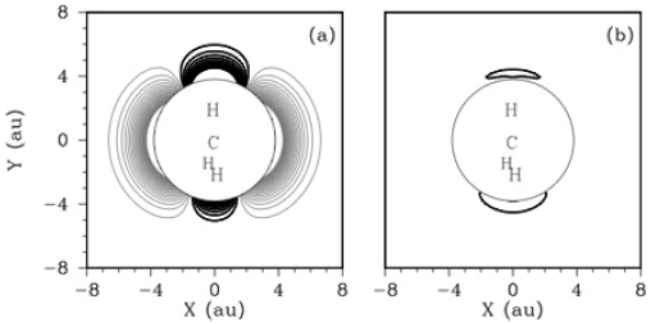

Figure 5. Corrected CASPT2/cc-pvdz potential surface and difference potentials for H + CH_3 → CH_4. Plotting conventions are as in Figure 4.

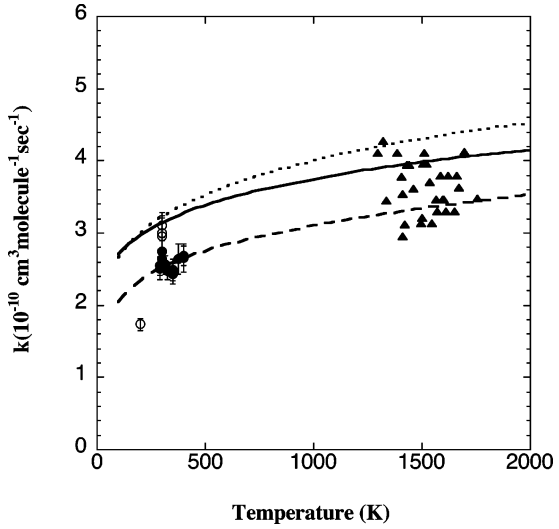

Figure 6. High-pressure-limit rate coefficients for H + CH_3 → CH_4. The solid curve is calculated using the CAS+1+2/aug-cc-pvtz potential, the dashed curve using the CASPT2/cc-pvdz potential, and the dotted curve using the corrected CASPT2/cc-pvdz potential. All of the calculated rates are multiplied by 0.9 to correct for recrossing. Key to experimental results: solid circles, Brouard et al.;[4] open circles, Seakins et al.;[1] solid triangles, Su and Michael.[5]

High-pressure-limit, TST rate coefficients from the CAS+1+2/aug-cc-pvtz, the CASPT2/cc-pvdz, and the corrected CASPT2/cc-pvdz potentials are shown in Figure 6. The rate coefficients from all three calculations are multiplied by 0.9 to correct for transition state recrossing (see above). As expected, the rate calculated on the uncorrected CASPT2/cc-pvdz potential is significantly below that on the CAS+1+2/aug-cc-pvtz potential because the CASPT2/cc-pvdz potential is less attractive. The error ranges from −25% at low temperature to −15% at high temperature. The rate calculated on the corrected CASPT2 potential is in significantly better agreement with the CAS+1+2/aug-cc-pvtz rate, having a maximum error of +5%.

Also shown in Figure 6 for comparison are experimentally derived rate coefficients.[1,4,5] The experimental measurements have all been made for isotopically substituted reactions and have been converted to high-pressure-limit H + CH_3 rate coefficients.[21] There is a fairly wide scatter in the experimental data, and our best calculations (solid and dotted lines) are seen to be in good agreement with the higher end of the experimental results.

For this reaction, it is possible to consider somewhat larger basis sets. The association rate coefficients calculated with the CAS+1+2 method employing the cc-pvdz, cc-pvtz, and cc-pvqz basis sets as well as the aug-cc-pvdz, aug-cc-pvtz, and aug-cc-pvqz basis sets are illustrated in Figure 7. As expected, both series appear to be converging, and the convergence appears to be to the same value. The corresponding one-dimensional reaction path potential energy curves show similar trends. Notably, the augmented basis sets converge much more rapidly, with the aug-cc-pvqz result essentially identical to the aug-cc-pvtz result.

3.1.2. H + C_2H_5 → C_2H_6. In Figure 8a, we show a two-dimensional contour plot of the CASPT2/cc-pvdz potential for hydrogen atom interacting with an ethyl radical. Unlike methyl radical, the radical site of the ethyl radical is slightly nonplanar making the front and back of the radical unequivalent. Although the front of the radical site is somewhat more attractive than the back, the potential surface clearly shows that barrierless additions from either side are possible. Also unlike H + CH_3,

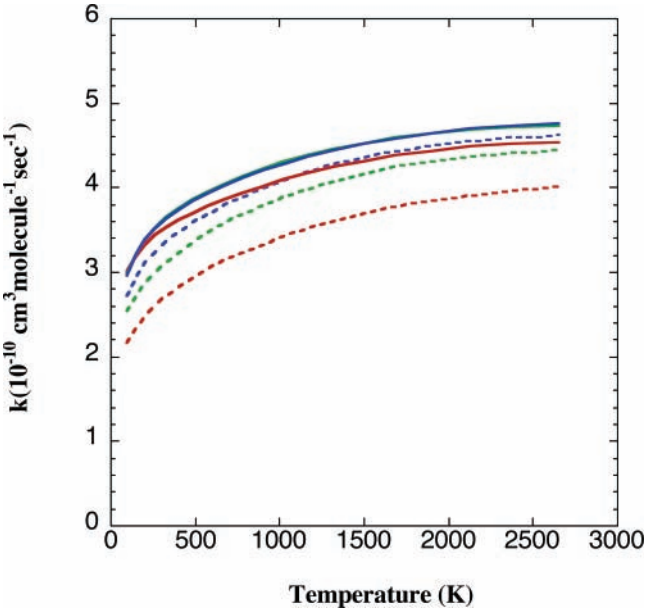

Figure 7. High-pressure-limit rate coefficients for H + CH_3 → CH_4: CAS+1+2/cc-pvdz (dashed red), CAS+1+2/cc-pvtz (dashed green), CAS+1+2/cc-pvqz (dashed blue), CAS+1+2/aug-cc-pvdz (solid red), CAS+1+2/aug-cc-pvtz (solid green), and CAS+1+2/aug-cc-pvqz (solid blue).

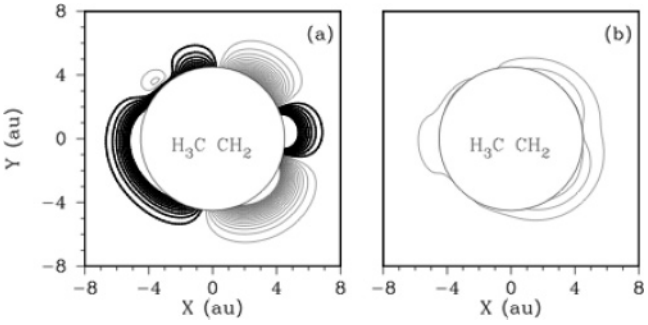

Figure 8. CASPT2/cc-pvdz potential surface and difference potentials for H + C_2H_5 → C_2H_6. The plotting plane is the symmetry plane. Plotting conventions are as in Figure 4.

H + C_2H_5 has a second strongly exothermic, product channel, abstraction or disproportionation, forming H_2 + ethylene. These calculations, in agreement with our previous calculations,[66] show a barrierless path for abstraction of one of the three methyl hydrogen atoms. In Figure 8a, this abstraction path appears as two negative contours in the upper-left quadrant. In our previous study, we concluded that addition is the dominant product channel with disproportionation contributing at most 15% at low temperature, rising to at most 40% at high temperature (but most likely still less than 15%). A complete treatment of the disproportionation path must take into account the relaxation of the geometry of the ethyl radical as the reaction progresses and, for this reason, is beyond the scope of this paper. For all systems studied here, we will focus only on the association reactions.

In Figure 8b, we show the difference potential (CAS+1+2/aug-cc-pvtz minus CASPT2/cc-pvdz) for the H + C_2H_5 association. As for H + CH_3, the difference potential is found to be small, and at least in the vicinity of the addition paths, it has little angle dependence. A plot of the corrected CASPT2 potential (eq 10) is shown in Figure 9a, and the difference between the corrected CASPT2/cc-pvdz potential and the CAS+1+2/aug-cc-pvtz potential is plotted in Figure 9b. The difference plot shows that on the CH_2 side of the radical the

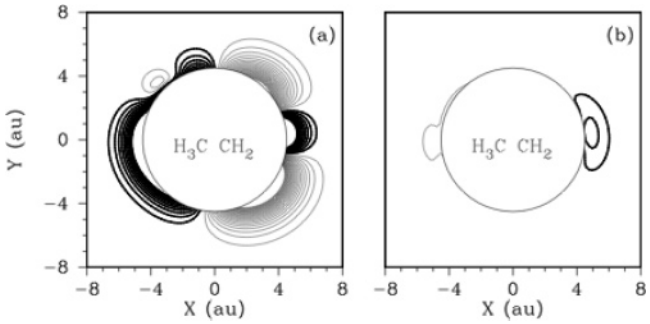

Figure 9. Corrected CASPT2/cc-pvdz potential surface and difference potentials for $H + C_2H_5 \rightarrow C_2H_6$. Plotting conventions are as in Figure 4.

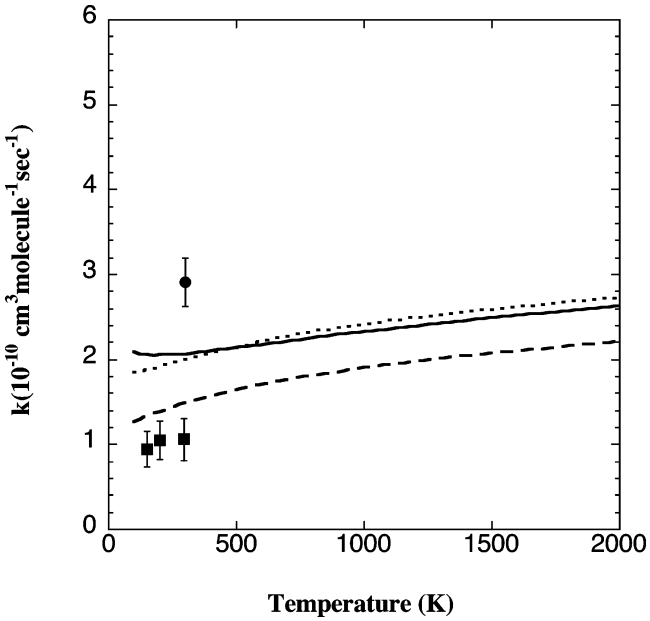

Figure 10. High-pressure-limit rate coefficients for $H + C_2H_5 \rightarrow C_2H_6$. Plotting conventions are as in Figure 6. The solid circle represents the experimental result of Sillesen et al.[49] The solid squares are the results of Pimentel et al.[50]

potential is a little too attractive (as was the case for $H + CH_3$), while on the CH_3 side the potential is still a little too repulsive. Again, as for $H + CH_3$, the largest errors occur in regions where the potential is repulsive and so should have little effect on the predictions for the association kinetics.

A comparison of the high-pressure-limit association rate coefficients on the three potentials is shown in Figure 10. The results are very similar to those for $H + CH_3$ with the uncorrected CASPT2 potential giving rate coefficients that are low by 10−40% relative to the CAS+1+2 potential, while the corrected CASPT2 and CAS+1+2 results are within ±10% over the entire temperature range.

Also shown in Figure 10 are the experimental results of Sillesen et al.[49] and Pimentel et al.,[50] the two most recently reported measurements. At room temperature, the predicted rate, 2.0×10^{-10} cm^3 $molecule^{-1}$ s^{-1} falls between the results from refs 49 (2.9×10^{-10} cm^3 $molecule^{-1}$ s^{-1}) and 50 (1.1×10^{-10} cm^3 $molecule^{-1}$ s^{-1}). The difference between the present theoretical result and the slightly higher rate of Sillesen et al.[49] might be explained in part by a contribution from the disproportionation channel, which is neglected in these calculations, although the only direct measurement[44] of the disproportionation rate suggests a contribution of just 2% to the total rate.

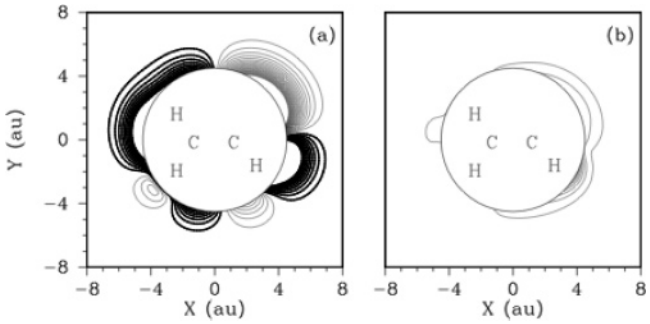

Figure 11. CASPT2/cc-pvdz potential surface and difference potentials for $H + C_2H_3 \rightarrow C_2H_4$. Plotting conventions are as in Figure 4. The plotting plane coincides with the C_2H_3 plane.

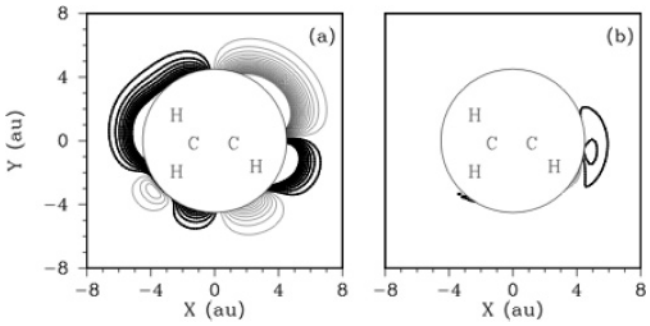

Figure 12. Corrected CASPT2/cc-pvdz potential surface and difference potentials for $H + C_2H_3 \rightarrow C_2H_4$. Plotting conventions are as in Figure 4.

3.1.3. $H + C_2H_3 \rightarrow C_2H_4$. In Figure 11a, we show a two-dimensional contour plot of the CASPT2/cc-pvdz potential for a hydrogen atom interacting with a vinyl radical. As for $H + C_2H_5$, there are two distinct barrierless addition paths corresponding to approach of the radical site from either the positive *y*-direction or the negative *y*-direction. In this case, the two addition paths are much less similar than for $H + C_2H_5$, with approach from the positive *y*-direction being much more attractive than approach from the negative *y*-direction. Also as for $H + C_2H_5$, there is a second exothermic, barrierless product channel corresponding to abstraction of one of the CH_2 hydrogens (the one trans to the radical orbital). As discussed in our previous paper,[65] a pathway can also be found for abstraction of the other CH_2 hydrogen, although this path is predicted to have a small barrier and therefore will not compete to a significant extent with the barrierless paths. Also as for $H + C_2H_5$, we will consider only the association reaction.

In Figure 11b, we show the difference potential (CAS+1+2/aug-cc-pvtz minus CASPT2/cc-pvdz) for the $H + C_2H_3$ association. As for the previous cases, the difference potential is found to be small, and at least in the vicinity of the addition paths, it has little angle dependence. A plot of the corrected CASPT2 potential (eq 10) is shown in Figure 12a, and the difference between the corrected CASPT2/cc-pvdz potential and the CAS+1+2/aug-cc-pvtz potential is plotted in Figure 12b. The difference plot shows that on the CH side of the radical (the right-hand side of the plot) the potential is a little too attractive, but again the largest errors are in regions where the potential is repulsive and so should have little effect on the association kinetics.

A comparison of the high-pressure-limit association rate coefficients on the three potentials is shown in Figure 13. The results are very similar to those for the previous reactions with the uncorrected CASPT2 potential giving rate coefficients that are low by 10−40% relative to the CAS+1+2 potential, while

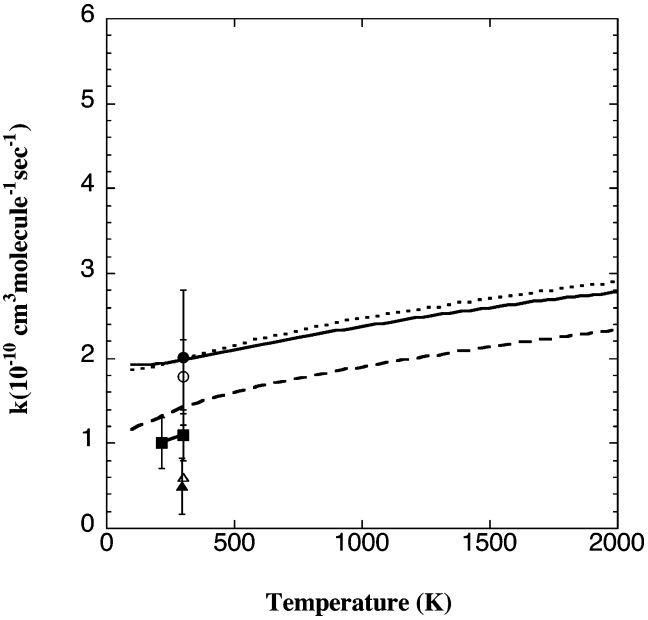

Figure 13. High-pressure-limit rate coefficientts for $H + C_2H_3 \rightarrow C_2H_4$. Plotting conventions are as in Figure 6. Key to experimental results: solid circle, Fahr et al.;[60] open circle, Fahr;[59] solid square, Monks et al.;[58] solid triangle, Heinemann et al.;[61] open triangle, Kowari et al.[62]

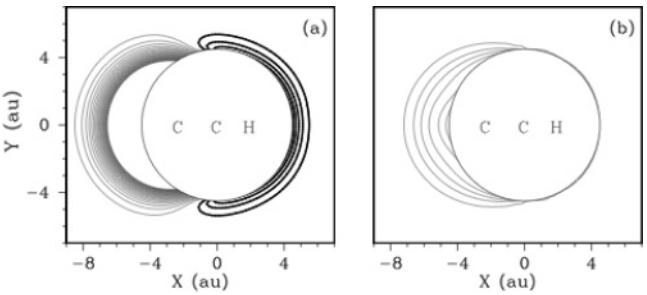

Figure 14. CASPT2/cc-pvdz potential surface and difference potentials for $H + CCH \rightarrow C_2H_2$. Plotting conventions are as in Figure 4.

the corrected CASPT2 and CAS+1+2 results are within ±10% over the entire temperature range.

Also shown in Figure 13 are the experimental data of Fahr et al.,[59,60] Monks et al.,[58] Heinemann et al.,[61] and Kowari et al.[62] The calculations agree well with the higher end of the range of experimental data. An estimated 10% contribution from disproportionation[65] does not significantly affect this comparison.

3.1.4. H + CCH → HCCH. In Figure 14a, we show a two-dimensional contour plot of the CASPT2/cc-pvdz potential for a hydrogen atom interacting with an ethynyl radical. In Figure 14b, we show the difference potential (CAS+1+2/aug-cc-pvtz minus CASPT2/cc-pvdz) for the H + CCH association. As for the previous cases, the difference potential is found to be small, and at least in the vicinity of the addition paths, it has little angle dependence. A plot of the corrected CASPT2 potential (eq 10) is shown in Figure 15a, and the difference between the corrected CASPT2/cc-pvdz potential and the CAS+1+2/aug-cc-pvtz potential is plotted in Figure 15b. The difference plot shows that the agreement between the corrected CASPT2/cc-pvdz and the CAS+1+2/aug-cc-pvtz potentials is nearly perfect.

A comparison of the high-pressure-limit association rate coefficients on the three potentials is shown in Figure 16. The results obtained using the corrected CASPT2 and CAS+1+2 potentials are in nearly perfect agreement over the entire

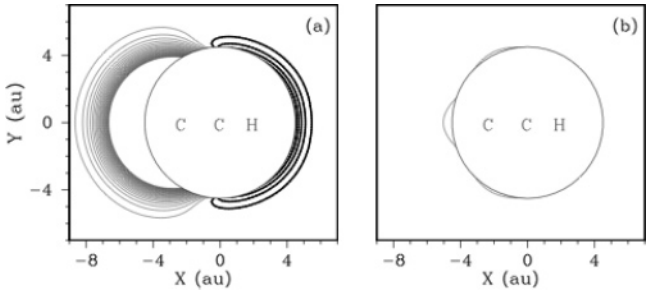

Figure 15. Corrected CASPT2/cc-pvdz potential surface and difference potentials for $H + CCH \rightarrow C_2H_2$. Plotting conventions are as in Figure 4.

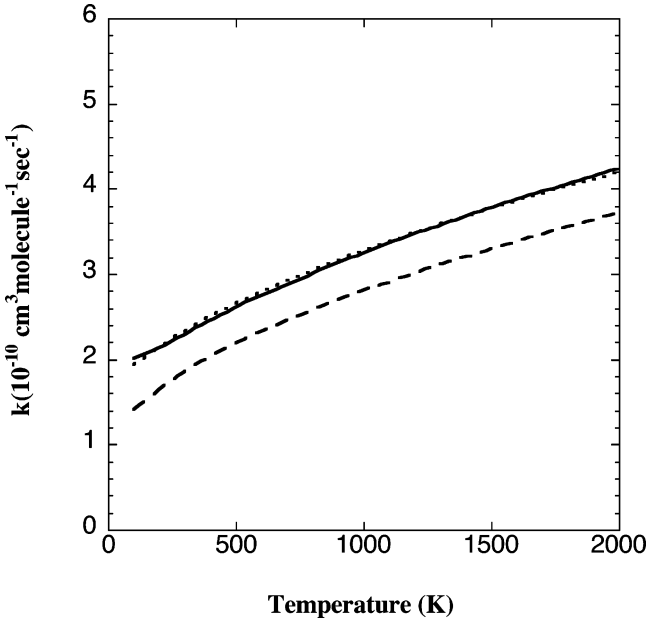

Figure 16. Computed high-pressure-limit VRC-TST rate coefficients for $H + CCH \rightarrow C_2H_2$. Plotting conventions are as in Figure 6.

temperature range, while the uncorrected CASPT2 results are again 10−30% too low.

3.2. Corrected CASPT2/cc-pvdz Calculations for Larger Systems. In the preceding section, it was demonstrated that VRC-TST calculations using corrected CASPT2/cc-pvdz potential surfaces yield association rate coefficients for all four test reactions, $H + CH_3$, $H + C_2H_5$, $H + C_2H_3$, and $H + C_2H$, that are in excellent agreement with results using more accurate (and much more costly) CAS+1+2/aug-cc-pvtz potential surfaces. Thus, although the 1D correction used is based only on the $H + CH_3$ reaction, it appears to be applicable to potential surfaces for H atom reactions with a wide range of hydrocarbon radicals. In this section, we report the results of calculations using the corrected CASPT2/cc-pvdz potentials on larger systems for which large basis set, multireference configuration interaction calculations are not feasible.

3.2.1. H + Alkyl Radicals. Corrected CASPT2/cc-pvdz potential surfaces for H + *iso*-propyl and H + *tert*-butyl are shown in Figure 17. Comparing these to the corresponding plots for $H + CH_3$ (Figure 5a) and $H + C_2H_5$ (Figure 9a), we find that the width of the attractive addition paths becomes narrower as more methyl substituents are placed around the radical site, consistent with standard theories of steric hindrance.[52] The effects on the high-pressure-limit association rate coefficients are shown in Figure 18, where we compare calculated rate coefficients for $H + CH_3$, $H + C_2H_5$, $H + iso\text{-}C_3H_7$, and $H + tert\text{-}C_4H_9$. The calculations predict a decrease in the association

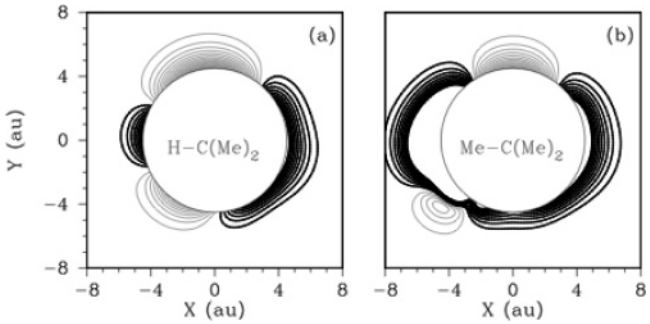

Figure 17. H + *iso*-C_3H_7 and H + *tert*-C_4H_9 potential surfaces. Plotting conventions are as in Figure 3. The plotting planes are the symmetry planes.

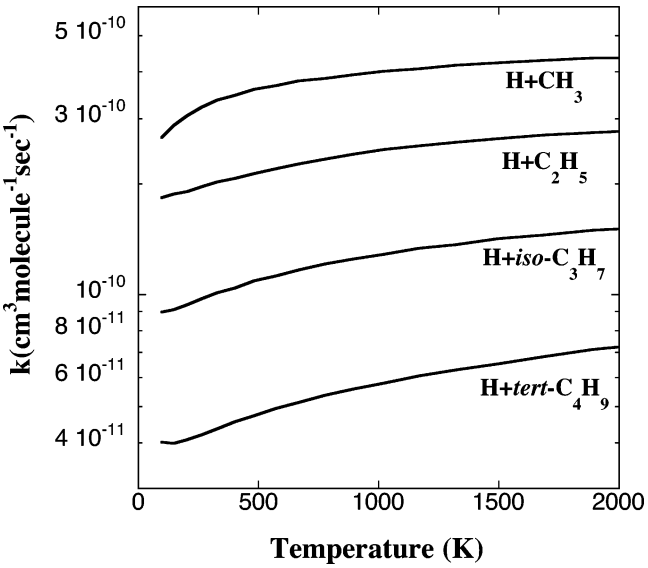

Figure 18. Computed high-pressure-limit VRC-TST rate coefficients for H + CH_3, H + C_2H_5, H + *iso*-C_3H_7, and H + *tert*-C_4H_9.

rate of approximately a factor of 2 for each additional methyl substituent. The temperature dependence of the four rate coefficients is remarkably similar with only the H + CH_3 rate having a slightly steeper temperature dependence at the low end of the temperature range studied.

In the previous section, the calculated rate coefficients for H + CH_3 and H + C_2H_5 were compared with available experimental results and found to be in reasonable agreement. For H + *iso*-C_3H_7, the only experimental result currently available is the room-temperature measurement by Munk et al.[51] ($(2.5 \pm 0.5) \times 10^{-10}$ cm^3 molecule^{-1} s^{-1}). This is approximately a factor of 2 higher than the calculated rate. Again, some of this difference might be attributable to the disproportionation reaction, which is not included in the calculations but may contribute to the observed *iso*-C_3H_7 depletion rate.

3.2.2. H + C_6H_5. The calculated and experimental rate coefficients for H + phenyl radical are shown in Figure 19. The experimental results[88−92] range from about 4.0×10^{-11} to 4.0×10^{-10} cm^3 molecule^{-1} s^{-1}. The calculated rate coefficient ranges from 1.6×10^{-10} cm^3 molecule^{-1} s^{-1} at room temperature to 1.9×10^{-10} cm^3 molecule^{-1} s^{-1} at 1000 K, which is well within the scatter of the experimental data. The calculated rate coefficient for H + phenyl is noticeably less than that for H + C_2H_3 (1.6×10^{-10} vs 2.1×10^{-10} cm^3 molecule^{-1} s^{-1} at room temperature). This can be explained by the fact that there are two barrierless addition paths for H + C_2H_3 (Figure 12a) but only one for H + phenyl.

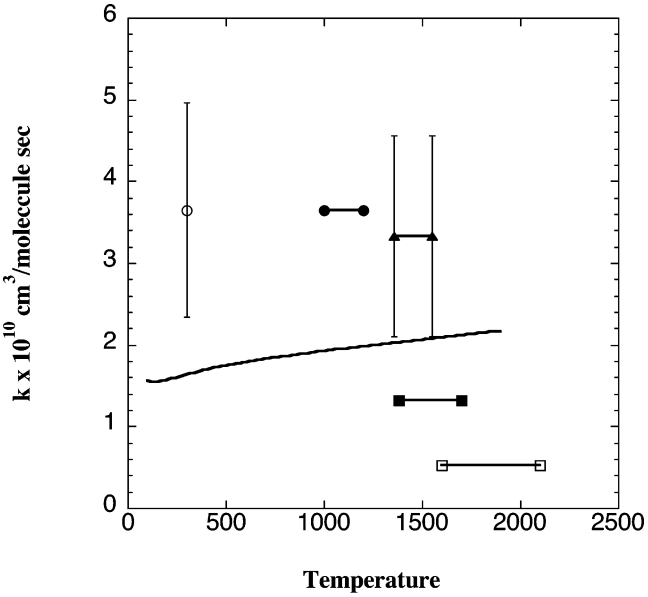

Figure 19. High-pressure-limit rate coefficients for H + C_6H_5. Key to experimental results: open circle, Ackermann et al.;[90] solid circles, Davis et al.;[91] solid squares, Braun-Unkhoff et al.;[89] open squares, Muller-Markgraf et al.;[88] solid triangles, Kumaran et al.[92]

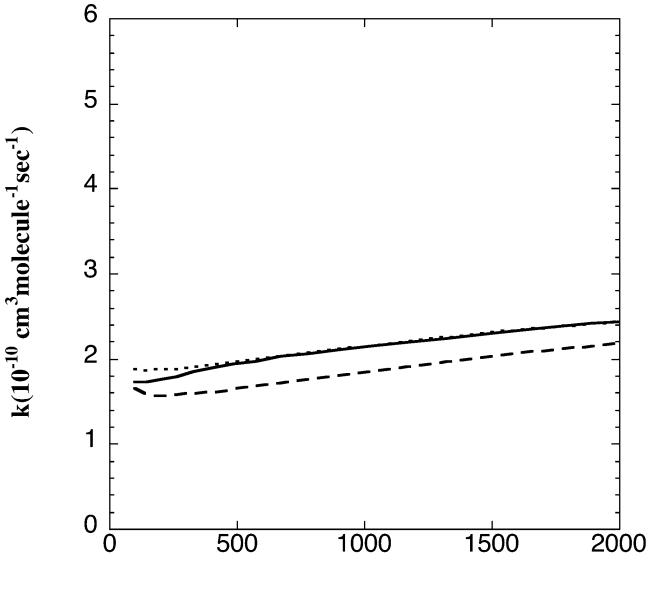

Figure 20. Computed high-pressure-limit VRC-TST rate coefficients for H + C_6H_5, H + 1-naphthyl, and H + 2-naphthyl. The solid line refers to H + C_6H_5, the dotted line to H + 1-naphthyl, and the dashed line to H + 2-naphthyl.

3.2.3. H + $C_{10}H_7$. The calculated rate coefficients for H reacting with 1-naphthyl and 2-naphthyl are shown in Figure 20 along with the rate for H + phenyl radical, for comparison purposes. No experimental results are available for H + naphthyl. The H + phenyl and H + 1-naphthyl rate coefficients are predicted to be virtually identical, while that for H + 2-naphthyl is only 15% lower. This implies that the steric factors for these three reactions are also nearly identical. Since the geometries of the three radical sites are similar, particularly for H + C_6H_5 and H + 1-naphthyl, and the character of the three radical orbitals are similar (all are sp^2), it should not be surprising that the steric factors would also be similar. One could reasonably speculate that the rate coefficients for hydrogen atom

reactions with other larger polycyclic aromatic hydrocarbon radicals will also be similar.

4. Concluding Remarks

The major conclusions from this study can be summarized as follows:

(1) CASPT2 vs CAS+1+2: Potential surfaces for radical−radical association reactions calculated with CASPT2 and CAS+1+2 calculations are found to be nearly indistinguishable. For this class of reactions, then it would appear that there is no advantage to using the more costly CAS+1+2 approach. There will likely be exceptions to this, most notably for radicals having degenerate or nearly degenerate ground states.

(2) Basis Set Effects: Potential surfaces calculated with the larger, aug-cc-pvtz basis set are significantly more attractive than those calculated with the smaller cc-pvdz basis set. The difference is large enough to have a noticeable (~20%) impact on association rate coefficients. However, the difference potentials (aug-cc-pvtz minus cc-pvdz) are found to be quite simple functions. A one-dimensional correction to the cc-pvdz potential surfaces (based on the H + CH_3 reaction) yields surfaces that, for the purposes of calculating association rate coefficients, are nearly indistinguishable from the full aug-cc-pvtz-based potentials.

(3) H + R Association Rate Coefficients: The calculated, high-pressure-limit H + R association rate coefficients for reactions 1−9 over the temperature range of 200−2000 K are well fit (±5%) by the following expressions

$$k_1 = 1.15 \times 10^{-10}\, T^{0.18}$$

$$k_2 = 9.04 \times 10^{-11}\, T^{0.16}$$

$$k_3 = 2.76 \times 10^{-11}\, T^{0.22}$$

$$k_4 = 8.64 \times 10^{-12}\, T^{0.28}$$

$$k_5 = 3.73 \times 10^{-11}\, T^{0.32}$$

$$k_6 = 6.45 \times 10^{-11}\, T^{0.20}$$

$$k_7 = 6.92 \times 10^{-11}\, T^{0.15}$$

$$k_8 = 8.08 \times 10^{-11}\, T^{0.13}$$

$$k_9 = 5.41 \times 10^{-11}\, T^{0.17}$$

where T is the temperature in K and the rate coefficients are in cm^3 $molecule^{-1}$ s^{-1}.

The rate coefficients vary by approximately 1 order of magnitude with H + CH_3 being the largest and H + *tert*-butyl the smallest. All of the H + R association rate coefficients are predicted to have small positive temperature dependences. The largest temperature dependences are for H + *tert*-butyl (reaction 4), and H + ethynyl (reaction 5), both of which are predicted to increase by ~30% from 300 to 1000 K. The smallest temperature dependence is for H + 1-naphthyl with a predicted increase of only 15% from 300 to 1000 K. Comparing the four reactions involving alkyl radicals, reactions 1−4, we find that each methyl substituent, adjacent to the radical site, lowers the association rate by approximately a factor of 2, i.e., $k_1 \approx 2k_2 \approx 4k_3 \approx 8k_4$.

We are currently exploring generalizations of this approach to other classes of reactions. For example, we have also used large basis set, multireference configuration interaction calculations for the $CH_3 + CH_3$ reaction to obtain a one-dimensional correction to CASPT2/cc-pvdz energies within VRC-TST kinetic estimates for a set of hydrocarbon radical−hydrocarbon radical association reactions.[93] Similar generalizations to the treatment of hydroperoxy radical reactions, for example, should be straightforward. We are also in the process of exploring extensions of this approach to the treatment of resonantly stabilized radicals such as propargyl.[94] The generalizations to radicals with degenerate (or nearly degenerate ground states), such as OH, alkoxy radicals, or halogen atoms, may suffer from limitations in the CASPT2 treatment of such degeneracies. Nevertheless, the increase in the splitting of the states at short separations may allow for the use of analogues of the present CASPT2/cc-pvdz-based approach in the exploration of the high-temperature regime of importance to combustion. For some reaction classes, it may be difficult to obtain suitable reference systems for obtaining the one-dimensional CAS+1+2/aug-cc-pvtz corrections. In this regard, it is worth noting that the CASPT2/cc-pvdz predictions are still within about 20% of the CAS+1+2/aug-cc-pvtz results for the four test systems studied here.

Acknowledgment. This work is supported by the Division of Chemical Sciences, Geosciences, and Biosciences, the Office of Basic Energy Sciences, the U. S. Department of Energy. The work at Argonne was supported under DOE Contract No. W-31-109-ENG-38. Sandia is a multiprogram laboratory operated by the Sandia Corporation, a Lockheed Martin Company, for the U. S. Department of Energy under Contract No. DE-AC04-94-AL85000.

References and Notes

(1) Seakins, P. W.; Robertson, S. H.; Pilling, M. J.; Wardlaw, D. M.; Nesbitt, F. L.; Thorn, R. P.; Payne, W. A.; Stief, L. J. *J. Phys. Chem. A* **1997**, *101*, 9974.
(2) Parkinson, C. D.; Griffioen, E.; McConnell, J. C.; Jaffel, L. B.; Vidal-Madjar, A.; Clarke, J. T.; Gladstone, G. R. *Geophys. Res. Lett*. **1999**, *26*, 3177.
(3) Cheng, J.-T.; Yeh, C.-T. *J. Phys. Chem*. **1977**, *81*, 1982.
(4) Brouard, M.; Macpherson, M. T.; Pilling, M. J. *J. Phys. Chem*. **1989**, *93*, 4047.
(5) Su, M.-C.; Michael, J. V. *Proc. Combust. Inst*. **2002**, *29*, 1219.
(6) Roth, P.; Just, Th. *Ber. Bunsen−Ges. Phys. Chem*. **1975**, *79*, 682.
(7) Klemm, R. B.; Sutherland, J. W.; Rabinowitz, M. J.; Patterson, P. M.; Quuartemont, J. M.; Tao, W. *J. Phys. Chem*. **1992**, *96*, 1786.
(8) Kiefer, J. H.; Kumaran, S. S. *J. Phys. Chem*. **1993**, *97*, 414.
(9) Davidson, D. F.; Di Rosa, M. D.; Chang, A. Y.; Hanson, R. K.; Bowman, C. T. *Proc. Combust. Inst.* **1992**, *24*, 589.
(10) Davidson, D. F.; Hanson, R. K.; Bowman, C. T. *Int. J. Chem. Kinet*. **1995**, *27*, 305.
(11) Sutherland, J. W.; Su, M.-C.; Michael, J. V. *Int. J. Chem. Kinet*. **2001**, *33*, 669.
(12) Duchovic, R. J.; Hase, W. L.; Schlegel, H. B.; Frisch, M. J.; Raghavachari, K. *Chem. Phys. Lett*. **1982**, *89*, 120.
(13) Hirst, D. M. *Chem Phys. Lett*. **1985**, *122*, 225.
(14) Hase, W. L.; Mondro, S. L.; Duchovic, R. J.; Hirst, D. M. *J. Am. Chem. Soc*. **1987**, *109*, 2916.
(15) Brown, F. B.; Truhlar, D. G. *Chem. Phys. Lett*. **1985**, *113*, 441.
(16) Schlegel, H. B. *J. Chem. Phys*. **1985**, *84*, 4530.
(17) Peyerimhoff, S. D.; Lewerenz, M.; Quack, M. *Chem. Phys. Lett*. **1984**, *109*, 563.
(18) Lewerenz, M.; Quack, M. *J. Chem. Phys*. **1988**, *88*, 5408.
(19) Furue, H.; Leblanc, J. F.; Pacey, P. D.; Whalen, J. M. *Chem. Phys.* **1991,** *154*, 425.
(20) Harding, L. B. *Ber. Bunsen−Ges. Phys. Chem*. **1997**, *101*, 363.
(21) Klippenstein, S. J.; Georgievskii, Y.; Harding, L. B. *Proc. Combust. Inst.* **2002**, *29*, 1229.
(22) Quack, M.; Troe, J. *Ber. Bunsen−Ges. Phys. Chem*. **1977**, *81*, 329.
(23) Quack, M. *J. Phys. Chem*. **1979**, *83*, 150.
(24) Cobos, C. J.; Troe, J. *Chem. Phys. Lett*. **1985**, *113*, 419.

(25) Cobos, C. J. *J. Chem. Phys*. **1986**, *85*, 5644.
(26) Troe, J. *J. Chem. Soc., Faraday Trans.* **1991**, *87*, 2299.
(27) Cobos, C. J. *Int. J. Chem. Kinet*. **1989**, *21*, 165.
(28) Stewart, P. H.; Smith, G. P.; Golden, D. M. *Int. J. Chem. Kinet*. **1989**, *21*, 923.
(29) Duchovic, R. J.; Hase, W. L.; Schlegel, H. B. *J. Chem. Phys*. **1984**, *88*, 1339.
(30) LeBlanc, J. F.; Pacey, P. D. *J. Chem. Phys*. **1985**, *83*, 4511.
(31) Aubanel, E. E.; Wardlaw, D. M. *J. Phys. Chem*. **1989**, *93*, 4511.
(32) Hu, X.; Hase, W. L. *J. Phys. Chem.* **1989**, *93*, 6029.
(33) Hu, X.; Hase, W. L. *J. Chem. Phys*. **1991**, *95*, 8073.
(34) Forst, W. *J. Phys. Chem*. **1991**, *95*, 3612.
(35) Takahashi, J.; Momose, T.; Shida, T. *Bull. Chem. Soc. Jpn*. **1994**, *67*, 74.
(36) Robertson, S. H.; Wagner, A. F.; Wardlaw, D. M. *J. Chem. Phys*. **1995**, *103*, 2917.
(37) Duchovic, R. J.; Hase, W. L. *Chem. Phys. Lett*. **1984**, *110*, 474.
(38) Duchovic, R. J.; Hase, W. L. *J. Chem. Phys*. **1985**, *82*, 3599.
(39) Hase, W. L.; Duchovic, R. J. *J. Chem. Phys*. **1985**, *83*, 3448.
(40) Mardis, K. L.; Sibert, E. L. *J. Chem. Phys*. **1998**, *109*, 8897.
(41) Kurlyo, M. J.; Peterson, N. C.; Braun, W. *J. Chem. Phys*. **1970**, *53*, 2276.
(42) Teng, L.; Jones, W. E. *J. Chem. Soc., Faraday Trans. 1* **1972**, *68*, 1267.
(43) Michael, J. V.; Osborne, D. T.; Suess, G. N. *J. Chem. Phys*. **1973**, *58*, 2800.
(44) Camilleri, P.; Marshall, R. M.; Purnell, J. H.; *J. Chem. Soc., Faraday Trans. 1* **1974**, *70*, 1434.
(45) Pratt, G. L.; Veltmann, I. *J. Chem. Soc., Faraday Trans. 1* **1974**, *70*, 1840.
(46) Pratt, G. L.; Veltmann, I. *J. Chem. Soc., Faraday Trans. 1* **1976**, *72*, 1733.
(47) Pacey, P. D.; Wimalasena, J. H. *Can. J. Chem*. **1984**, *62*, 293.
(48) Pratt, G. L.; Wood, S. W. *J. Chem. Soc., Faraday Trans. 1* **1984**, *80*, 3419.
(49) Sillesen, A.; Ratajczak, E.; Pagsberg, P. *Chem. Phys. Lett.* **1993**, *201*, 171.
(50) Pimentel, A. S.; Payne, W. A.; Nesbitt, F. L.; Cody, R. J.; Stief, L. J. *J. Phys. Chem. A* **2004**, *108*, 7204.
(51) Munk, J.; Pagsberg, P.; Ratajczak, E. Sillesen, A. *Chem. Phys. Lett*. **1986**, *132*, 417.
(52) Benson, S. W. *Can. J. Chem*. **1983**, *61*, 881.
(53) Kruse, T.; Roth, P. *J. Phys. Chem. A* **1997**, *101*, 2138.
(54) Wu, C. H.; Singh, H. J.; Kern, R. D. *Int. J. Chem. Kinet*. **1987**, *19*, 975.
(55) Frank, P.; Just, Th. *Combust. Flame* **1980**, *38*, 231.
(56) Wagner, A. F.; Harding, L. B. Robertson, S. H.; Wardlaw, D. M. *Ber. Bunsen−Ges. Phys. Chem*. **1997**, *101*, 391.
(57) Kiefer, J. H.; Mudipalli, P. S.; Wagner, A. F.; Harding, L. B. *J. Chem. Phys*. **1996**, *105*, 8075.
(58) Monks, P. S.; Nesbitt, F. L.; Payne, W. A.; Scanon, M.; Stief, L. J.; Shallcross, D. E. *J. Phys. Chem.* **1995**, *99*, 17151.
(59) Fahr, A. *Int. J. Chem. Kinet*. **1995**, *27*, 769.
(60) Fahr, A.; Laufer, A.; Klein, R.; Braun, W. *J. Phys. Chem*. **1991**, *95*, 3218.
(61) Heinemann, P.; Hofmann-Sievert, R.; Hoyermann, K. *Proc. Combust. Inst.* **1988**, *21*, 865.
(62) Kowari, K.; Sugawara, K.; Sato, S.; Nagase, S. *Bull. Chem. Soc. Jpn*. **1981**, *54*, 1222.
(63) Laufer, A. H.; Fahr, A. *Chem. Rev.* **2004**, *104*, 2813.
(64) Kiefer, J. H.; Santhanam, S.; Srinivasan, N. K.; Tranter, R. S.; Klippenstein, S. J.; Oehlschlaeger, M. A. *Proc. Combust. Inst.* **2005**, *30*, 1129.
(65) Klippenstein, S. J.; Harding, L. B. *Phys. Chem. Chem. Phys.* **1999**, *1*, 989.
(66) Harding, L. B.; Klippenstein, S. J. *Proc. Combust. Inst.* **1998**, *27*, 151.
(67) Klippenstein, S. J. *J. Chem. Phys.* **1992**, *96*, 367. Klippenstein, S. J. *Chem. Phys. Lett.* **1993**, *214*, 418. Klippenstein, S. J. *J. Phys. Chem*. **1994**, *98*, 11459.
(68) Georgievskii, Y.; Klippenstein, S. J. *J. Chem. Phys.* **2003**, *118*, 5442.
(69) Georgievskii, Y.; Klippenstein, S. J. *J. Phys. Chem. A* **2003**, *107*, 9776.
(70) Kendall, R. A., Dunning, T. H., Jr., Harrison, R. J. *J. Chem. Phys.* **1992**, *96*, 6796.
(71) Werner, H.-J.; Knowles, P. J. *J. Chem. Phys.* **1988**, *89*, 5803.
(72) Knowles, P. J.; Werner, H.-J. *Chem. Phys. Lett*. **1988**, *145*, 514.
(73) Dunning, T. H., Jr. *J. Chem. Phys*. **1989**, *90*, 1007.
(74) Celani, P.; Werner, H.-J. *J. Chem. Phys*. **2000**, *112*, 5546.
(75) Werner, H.-J.; Knowles, P. J.; Almlof, J.; Amos, R. D.; Berning, A.; Cooper, D. L.; Deegan, M. J. O.; Dobbyn, A. J.; Eckert, F.; Elbert, S. T.; Hampel, C.; Lindh, R.; Lloyd, A. W.; Meyer, W.; Nicklass, A.; Peterson, K.; Pitzer, R.; Stone, A. J.; Taylor, P. R.; Mura, M. E.; Pulay, P.; Schutz, M.; Stoll, H.; Thorsteinsson, T. *MOLPRO*, version 2002.6; University of Birmingham, U. K.
(76) Werner, H.-J.; Knowles, P. J. *J. Chem. Phys.* **1985**, *82*, 5053. Knowles, P. J., Werner, H.-J. *Chem. Phys. Lett*. **1985**, *115*, 259.
(77) Frisch, M. J.; Trucks, G. W.; Schlegel, H. B.; Scuseria, G. E.; Robb, M. A.; Cheeseman, J. R.; Zakrzewski, V. G.; Montgomery, J. A., Jr.; Stratmann, R. E.; Burant, J. C.; Dapprich, S.; Millam, J. M.; Daniels, A. D.; Kudin, K. N.; Strain, M. C.; Farkas, O.; Tomasi, J.; Barone, V.; Cossi, M.; Cammi, R.; Mennucci, B.; Pomelli, C.; Adamo, C.; Clifford, S.; Ochterski, J.; Petersson, G. A.; Ayala, P. Y.; Cui, Q.; Morokuma, K.; Malick, D. K.; Rabuck, A. D.; Raghavachari, K.; Foresman, J. B.; Cioslowski, J.; Ortiz, J. V.; Stefanov, B. B.; Liu, G.; Liashenko, A.; Piskorz, P.; Komaromi, I.; Gomperts, R.; Martin, R. L.; Fox, D. J.; Keith, T.; Al-Laham, M. A.; Peng, C. Y.; Nanayakkara, A.; Gonzalez, C.; Challacombe, M.; Gill, P. M. W.; Johnson, B. G.; Chen, W.; Wong, M. W.; Andres, J. L.; Head-Gordon, M.; Replogle, E. S.; Pople, J. A. *Gaussian 98*, revision A.7; Gaussian, Inc.: Pittsburgh, PA, 1998.
(78) Klippenstein, S. J. In *The Chemical Dynamics and Kinetics of Small Radicals*; Advances in Physical Chemistry 6; Liu, K., Wagner, A. F., Eds.; World Scientific: River Edge, NJ, 1995; Part 1, p 120. Truhlar, D. G.; Garrett, B. C.; Klippenstein, S. J. *J. Phys. Chem.* **1996**, *100*, 12771.
(79) Robertson, S.; Wagner, A. F.; Wardlaw, D. M. *J. Chem. Phys*. **2000**, *113*, 2648. Robertson, S. H.; Wardlaw, D. M.; Wagner, A. F. *J. Chem. Phys*. **2002**, *117*, 593.
(80) Robertson, S.; Wagner, A. F.; Wardlaw, D. M. *J. Phys. Chem. A* **2002**, *106*, 2598.
(81) Smith, S. C. *J. Chem. Phys*. **1999**, *111*, 1830. Smith, S. C. *J. Phys. Chem. A* **2000**, *104*, 10489.
(82) Klippenstein, S. J.; Harding, L. B. *Proc. Comb. Inst.* **2000**, *28*, 1503.
(83) Thiesemann, H.; Clifford, E. P.; Taatjes, C. A.; Klippenstein, S. J. *J. Phys. Chem. A* **2001**, *105*, 5393.
(84) Klippenstein, S. J.; Khundkar, L. R.; Zewail, A. H.; Marcus, R. A. *J. Chem. Phys.* **1988**, *89*, 4761.
(85) Klippenstein, S. J.; Marcus, R. A. *J. Chem. Phys.* **1990**, *93*, 2418.
(86) This assumption is valid when the internal coordinates have distinct well-separated minima corresponding to the front and back. Otherwise, one must resort to a fully anharmonic evaluation of the internal mode(s) partition function, which would lead to equivalent front and back contributions.
(87) Harding, L. B.; Klippenstein, S. J.; Georgievskii, Y. *Proc. Comb. Inst.* **2005**, *30*, 985.
(88) Muller-Markgraf, W.; Troe, J. *J. Phys. Chem*. **1988**, *92*, 4914.
(89) Braun-Unkhoff, M.; Frank, P.; Just, Th. *Proc. Combust. Inst*. **1989**, *22*, 1053.
(90) Ackermann, L.; Hippler, H.; Pagsberg, P.; Reihs, C.; Troe, J. *J. Phys. Chem*. **1990**, *94*, 5247.
(91) Davis, S. G.; Wang, H.; Brezinsky, K.; Law, C. K. *Proc. Combust. Inst*. **1996**, *26*, 1025.
(92) Kumaran, S. S.; Michael, V. V. *Int. Symp. Shock Waves, 20th, 1995* **1996**, *21*, 6510.
(93) Klippenstein, S. J.; Georgievskii, Y.; Harding, L. B., to be submitted for publication.
(94) Klippenstein, S. J.; Georgievskii, Y.; Harding, L. B. Unpublished work, 2005.